

Ballistic accretion on a point seed

S. RAMBALDI ⁽¹⁾, G. SALUSTRI ⁽¹⁾, F. PORCÚ ⁽²⁾ and F. PRODI ⁽²⁾⁽³⁾

⁽¹⁾ *Dipartimento di Fisica, Università di Bologna - Via Irnerio 46, 40126 Bologna, Italy*

⁽²⁾ *Istituto FISBAT/CNR, Gruppo Nubi e Precipitazioni - Via Gobetti 101, 40129 Bologna, Italy*

⁽³⁾ *Dipartimento di Fisica, Università di Ferrara - Via Paradiso 12, 44100 Ferrara, Italy*

(ricevuto il 25 Luglio 1996; approvato il 23 Settembre 1996)

Summary. — We carefully discuss the two-dimensional ballistic aggregation process. Studying the microscopic discrete process, we theoretically derive the probability density function describing the single-particle accretion. Using this function, we describe the properties of the “fan”, obtained for ballistic aggregation on the single seed, and we predict its mean density and its opening angle. We discuss the shadowing effect on a microscopic scale, between the single particles and, on a larger scale, between grown structures, deriving the columnar microstructure direction law. Comparisons with numerical experiments are shown.

PACS 92.60.Jq – Water in the atmosphere (humidity, clouds, evaporation, precipitation).

PACS 68.70 – Whiskers and dendrites (growth, structure, and nonelectronic properties).

1. – Introduction

In seed accretion problems, objects are produced from the subsequent aggregation of elementary units, subject to different motions (gravitational, chaotic, diffusive). Theoretical deterministic studies of these phenomena are not feasible for the high number of variables involved. Interesting results have been obtained with statistical studies of numerical simulations.

The very first numerical models were pure ballistic [1] or diffusion-limited [2]; later models have been adjusted to specific problems (thin-film growths, colloidal aggregates, atmospheric-ice growth, electrical deposits). Ramanlal and Sander [3], Limaye and Amritkar [4] and Rambaldi *et al.* [5], following different statistical techniques, explain some aggregates features (growing angle, mean density) theoretically, in agreement with values obtained from numerical simulations. Liang and Kadanoff [6] and Porcú and Prodi [7] show scaling properties of structures produced by aggregation.

Ballistic models have been used profitably to study atmospheric ice formation, due to aggregation of supercooled droplets. Atmospheric-ice deposits are found on artificial

structures, relative ly moving with respect to a supercooled droplet cloud: for example, ice deposits are found on electric wires, sea platforms, ships, metallic structures, aircraft portions, etc. Ice deposit features (size, shape, density) depend on atmospheric conditions. The pioneer paper of Buser and Aufdermaur [8] shows that a tridimensional pure ballistic simulation gives aggregates with realistic density. Ballistic models have been used from cloud physicists to study the atmospheric ice growth and the resulting precipitation element formation (graupel, hailstones). Improved ballistic models, with mechanical, hydrodynamic and thermodynamic effects, simulate field and laboratory results, see Prodi *et al.* [9], Porcú *et al.* [10], Lozowski *et al.* [11, 12], Szilder [13], with good agreement.

The pure ballistic model proves to be basic to understand atmospheric-ice deposits grown at “low density regime”, see Prodi *et al.* [14]. With “low density regime” we mean in the presence of low-speed droplets hitting a low-temperature seed, so that the droplets freeze immediately at contact.

In this paper we focus our attention on the basic mechanisms underneath two-dimensional ballistic aggregation on a point seed. This simple but realistic problem contains all the accretion mechanisms. The first part of this paper develops a theory predicting the opening angle of the growing aggregate, which results to be in good agreement with the outcomes of a two-dimensional ballistic numerical model; the second part extends the theoretical reasoning to the interior of the aggregate, considering the influence of close-by particles to give a theoretical upper bound to the mean density value. Then in the final section, through simple geometrical arguments, we derive a law predicting the slope of air inclusion channels in the aggregates. The analytical results described in the present paper have been verified by numerical simulations.

2. – Numerical model

We consider particles of different shapes, moving on a two-dimensional plane. We compute the motion of these particles, assuming they start far from the aggregate with initial positions uniformly random distributed and they all move on straight parallel lines without being affected by any fluid motion or turbulence. We further assume that, when a particle hits the aggregate, it freezes in that position, becomes part of the aggregate and the positions of all other particles of the aggregate are not modified by this process of accretion.

Figure 1 shows a graphic comparison of the accretion of a seed, obtained with circular and square particles. Through an ensemble average of 10^4 evolutions, each of them similar to the one shown in fig. 1, we find values of 26 and 33 degrees for the opening angles of square and circular particles, respectively. How to determine the “mean” opening angle of numerical aggregates will be discussed later, together with the mean density.

To understand how the aggregate opens up, we study the accretion process of its boundary. Let us consider a particle P on the left boundary of the aggregate. The opening angle θ is determined by the average position of the particles, aggregating on the particle P .

In the following pages we work with square particles, then we extend our results to circular particles, each one having a diameter equal to the side of the square particles. This can be easily done in two dimensions, because we consider a ballistic aggregation

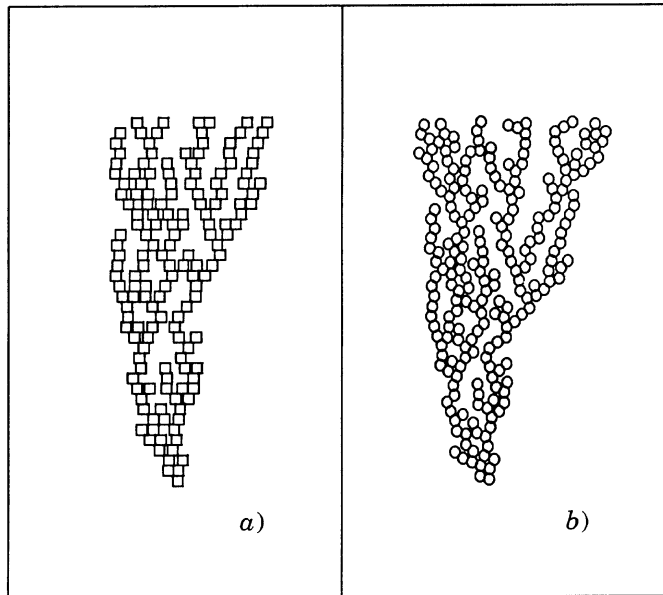


Fig. 1. - Numerical evolution of a ballistic accretion on a point seed, using square particles (a) and circular particles (b).

of particles that all move on straight parallel lines and because both square and circular particles have the same cross-section; this can be seen in fig. 1, where the two aggregates are generated from the same particle sequence. We notice that each particle has a different vertical coordinate, but it retains the same horizontal coordinate and it touches exactly the same particles.

To further simplify our discussion, in this section we consider square particles, of side l , moving on a lattice, of grid size d , equal to half the square side, $l/d = 2$, (see fig. 2). The lattice will be used only in this Section.

As falling particles are uniformly random distributed, the three configurations of fig. 2 have the same likelihood; if only these configurations existed, the average position of the new particle would be the same as P and the aggregate would not open up.

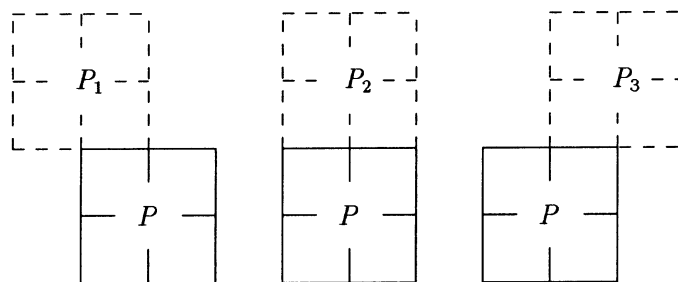


Fig. 2. - Possible accretions of particle P .

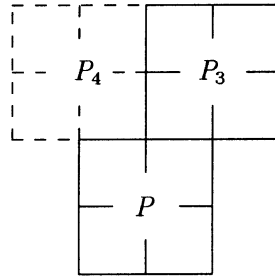


Fig. 3. – Possible accretion of particle P , once particle P_3 is in place.

The reason why it opens up is that, once particle P_3 is in place, a new particle P_4 , see fig. 3, can still get to its left side and now this new particle becomes the extreme left side of the aggregate. It follows that the probability of P_3 to be the extreme left side of the aggregate is smaller than the probability of P_2 which, in turn, is smaller than the probability of P_1 ; therefore the average position of the new particle, forming the extreme left side of the aggregate above P , is on the left of P .

3. – Theoretical model

To quantify our discussion on the opening angle, we use now an off-lattice continuous model with square particles; the choice of square particles has been previously justified and will be extended to circular particles later on.

To compute the probability of a particle to aggregate, we must take into account several possibilities. As we have already seen, the particle hitting P on its left boundary

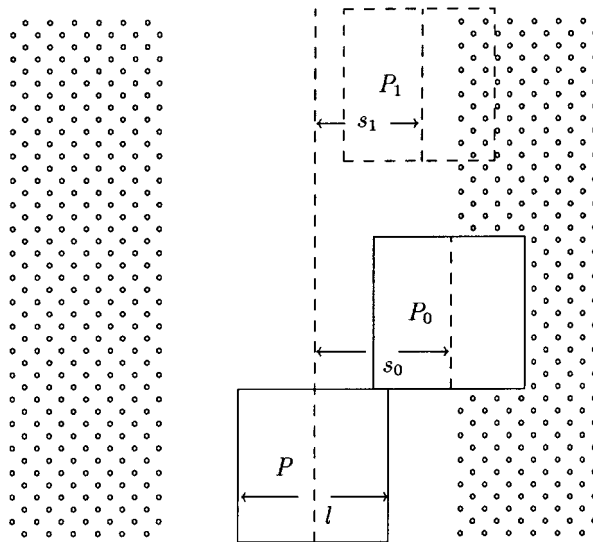


Fig. 4. – Fall of a particle P_1 partially shadowing P , once particle P_0 is in place, with $s_0 \geq 0$.

may be the first falling particle or the second or any following one. All these particles have different probabilities and we must consider all of them.

We consider the first particle hitting P and we recall the uniform random distribution of the falling particles; the probability density that the orthogonal projection of the center of this first added particle is at a distance s_0 from the orthogonal projection of the center of the particle P , with $-l < s_0 < +l$, is a constant, $\mathcal{P}_0 = 1/2l$, independent of the value of s_0 .

If s_0 is less than or equal to zero, then the extreme left side of the aggregate is formed, but if s_0 is greater than zero, we will consider the next falling particle, calling s_1 the distance between the orthogonal projection of the center of this new falling particle and the orthogonal projection of the center of particle P . The situation for $s_0 > 0$ is shown in fig. 4. In this case we want to know the probability that a new particle will hit P on the left of P_0 . Only particles with centers in the stripe of fig. 4 can influence this probability; they can hit P , if $-l < s_1 < s_0 - l$, and become the extreme left side of the aggregate, or they can hit P_0 and completely shadow P , if $s_0 - l < s_1 < 0$, and in this case P_0 is the extreme left side of the aggregate, or they can hit P_0 and partially shadow P , if $0 < s_1 < s_0$, and leave some room for a new particle to hit P . The probability for this second falling particle to hit one of these three regions is proportional to the width of these regions and it is, respectively, given by

$$\mathcal{P}_0 \frac{s_0}{s_0 + l}, \quad \mathcal{P}_0 \frac{l - s_0}{s_0 + l}, \quad \mathcal{P}_0 \frac{s_0}{s_0 + l}.$$

Again if $s_1 > 0$, we consider the next falling particle. This argument can be carried on to include infinite new particles and we can write

$$\mathcal{P}_0 \left\{ \begin{array}{l} \frac{s_0}{s_0 + l}, \\ \frac{l - s_0}{s_0 + l}, \\ \frac{s_0}{s_0 + l} \left\{ \begin{array}{l} \frac{1}{s_0} \int_0^{s_0} \frac{s_1}{s_1 + l} ds_1, \\ \frac{1}{s_0} \int_0^{s_0} \frac{l - s_1}{s_1 + l} ds_1, \\ \frac{1}{s_0} \int_0^{s_0} \frac{s_1}{s_1 + l} \left\{ \begin{array}{l} \frac{1}{s_1} \int_0^{s_1} \frac{s_2}{s_2 + l} ds_2, \\ \frac{1}{s_1} \int_0^{s_1} \frac{l - s_2}{s_2 + l} ds_2, \\ \frac{1}{s_1} \int_0^{s_1} \frac{s_2}{s_2 + l} (\dots) ds_2, \end{array} \right. ds_1, \end{array} \right. \end{array} \right.$$

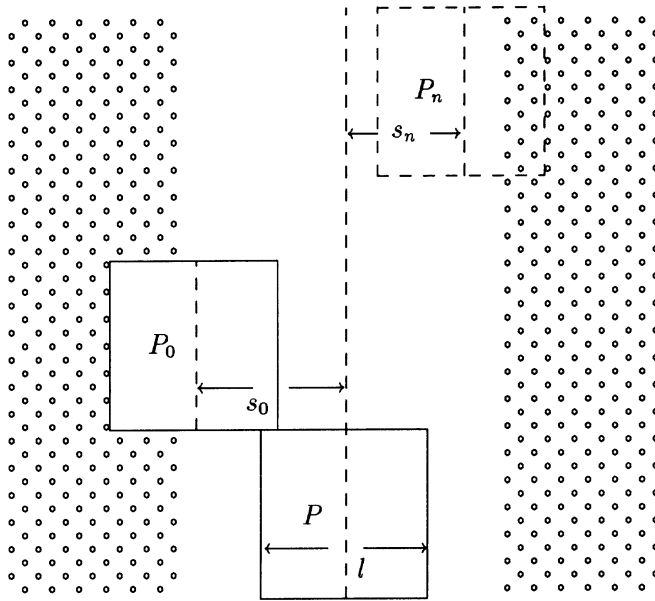


Fig. 5. - Fall of a particle P_n going to hit P , once particle P_0 is in place, with $s_0 < 0$.

where all terms in higher positions of parentheses represent the probabilities of particles hitting P , all terms in central positions represent the probabilities of particles completely shadowing P and all terms in lower positions represent the probabilities of particles partially shadowing P . Adding all terms describing direct impacts on P , we find that the probability of hitting again P , after a particle hits P at a distance s_0 , is given by

$$\begin{aligned} \underline{\mathcal{P}}(s_0) &= \frac{s_0}{s_0 + l} \left\{ 1 + \frac{1}{s_0} \int_0^{s_0} \frac{s_1}{s_1 + l} \left(1 + \frac{1}{s_1} \int_0^{s_1} \frac{s_2}{s_2 + l} (\dots) ds_2 \right) ds_1 \right\} = \\ &= \frac{s_0}{s_0 + l} \left\{ 1 + \sum_{m=1}^{\infty} \left(1 - \frac{l}{s_0} \left(\sum_{n=1}^m \frac{1}{n!} \left(\ln \frac{l + s_0}{l} \right)^n \right) \right) \right\} = \\ &= \frac{s_0}{s_0 + l} \left\{ 1 + \frac{l}{s_0} \sum_{m=1}^{\infty} \left(\sum_{n=m+1}^{\infty} \frac{1}{n!} \left(\ln \frac{l + s_0}{l} \right)^n \right) \right\} = \frac{s_0}{s_0 + l} + \frac{1}{2} \left(\ln \frac{l + s_0}{l} \right)^2. \end{aligned}$$

Removing the contributions of all these particles, we find that the probability density for a particle to hit P at a distance s , with $s > 0$, and from the extreme left side of the aggregate, is given by

$$\underline{\mathcal{P}}(s) = \underline{\mathcal{P}}_0 (1 - \underline{\mathcal{P}}(s)) \quad s \geq 0.$$

To derive $\underline{\mathcal{P}}(s)$, if $s < 0$, we consider the situation shown in fig. 5. For any realization with a particle P_0 already in place over P at a distance s_0 , there is a family of similar realizations with a particle hitting P at a distance s_n , with $s_0 + l < s_n < l$; it follows that the probability of hitting P at a distance s_n , after a particle has hit P at a

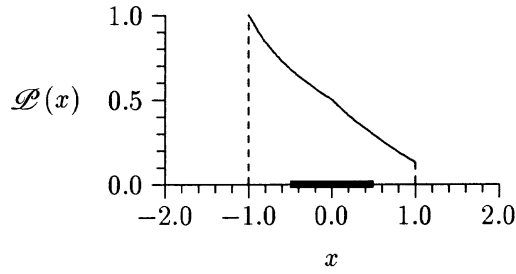


Fig. 6. - $\mathcal{P}(x)$ represents the probability density function of a particle to hit the left boundary of the “fan” (dark segment) in x and to become the new left boundary.

distance s_0 , is the same for any s_n , with $s_0 + l < s_n < l$. Using this property together with the conservation of particles, the probability $\overline{\mathcal{P}}(s)$ of hitting at a distance s , after a particle has hit P at any distance s_0 , is

$$\overline{\mathcal{P}}(s) = -s \frac{d}{ds} (\mathcal{P}(s+l)) = -\frac{s}{2l+s} \left(\frac{l}{2l+s} + \ln \frac{2l+s}{l} \right).$$

Adding the contributions of all these particles, the probability density that a particle hits P at a distance s , with $s < 0$, and forms the left boundary of the aggregate, is given by

$$\mathcal{P}(s) = \mathcal{P}_0 (1 + \overline{\mathcal{P}}(s)) \quad s < 0.$$

Introducing the new variable $x = s/l$, the probability density function can be rewritten as:

$$\mathcal{P}(x) = \begin{cases} 0.5 \left(\frac{1}{1+x} - 0.5 (\ln(1+x))^2 \right) & 0 \leq x \leq 1 \\ 0.5 \left(1 - \frac{x}{2+x} \left(\frac{1}{2+x} + \ln(2+x) \right) \right) & -1 \leq x < 0. \end{cases}$$

This function, shown in fig. 6, agrees with the results of an ensemble average of 10^6 numerical simulations with differences on the fourth decimal place.

We notice that $\int_{-1}^{+1} \mathcal{P}(x) dx = 1$; this means that, in our model, a new particle always hits the external particle forming the frontier. This implies that the new frontier is always connected with the old frontier and never comes from a branch starting in the interior of the aggregate. The growth probability is higher on the left, as expected (we are considering the left boundary) and, in particular, the middle position of the aggregating particle is given by

$$\langle x \rangle = \int_{-1}^{+1} x \mathcal{P}(x) dx = -0.27.$$

In the case of square particles, $\langle y \rangle = 1$, this implies a growth angle

$$\theta = \arctg \frac{\langle x \rangle}{\langle y \rangle} = 30.2^\circ.$$

This result can be extended to the case of circular particles; we consider circular particles with a diameter equal to the side of square particles. As all falling particles move on straight parallel lines, these circular particles move and shade exactly as their corresponding square particles (they have the same cross-section); only the aggregating position along the y -axis changes; in particular we have

$$\langle y \rangle = \int_{-1}^{+1} \sqrt{1-x^2} \mathcal{G}(x) dx = 0.78,$$

which brings to a growth angle $\theta = 38.3^\circ$. We notice that the high value of the x variance

$$\sqrt{\langle (x - \langle x \rangle)^2 \rangle} = \sqrt{\int_{-1}^{+1} (x - \langle x \rangle)^2 \mathcal{G}(x) dx} = 0.52,$$

similar to the variance measured in numerical simulations, justifies the need of ensemble averages over huge sets of realizations.

The average opening angle computed from the mean displacement of the boundary, for square particles, has the value of 30.2 degrees, to be compared with the value of 26.6 degrees, obtained with ensemble averages of numerical accretions, while the value of the opening angle for circular particles is 38.3 degrees, compared with the value of 33.6 degrees computed with the numerical model.

These differences are mainly due to the fact that some branches of the aggregate forming the boundary stop growing and the new boundary is formed by a branch directly coming from the interior of the aggregate. This event, present in the numerical evolutions, is not included in our theoretical model and leads to consistent larger estimates of the opening angle. Numerical computations show that, over a thousand cases, the boundary of the aggregate is formed by a branch connected with a particle of the previous boundary in 955 cases, by a branch connected with the first internal particle in 43 cases and by a branch connected with a more internal particle only in 2 cases.

Our theoretical model is based on the calculation of the angular probability distribution of particles aggregating to a given one. Our analytical study of this distribution leads to an overestimate of the fan opening angle of the original seed.

An interesting theoretical paper by Joag *et al.* [15] estimates the fan opening angle with a quite different approach; they study the probability distribution of the lengths of particles chains (fingers), in particular the number of particles lying between a point on the boundary and the next further boundary point.

4. - Growth in the interior

In the preceding sections, we have discussed the microscopic laws determining the opening of the accretion on a seed. In this section, we describe, by numerical

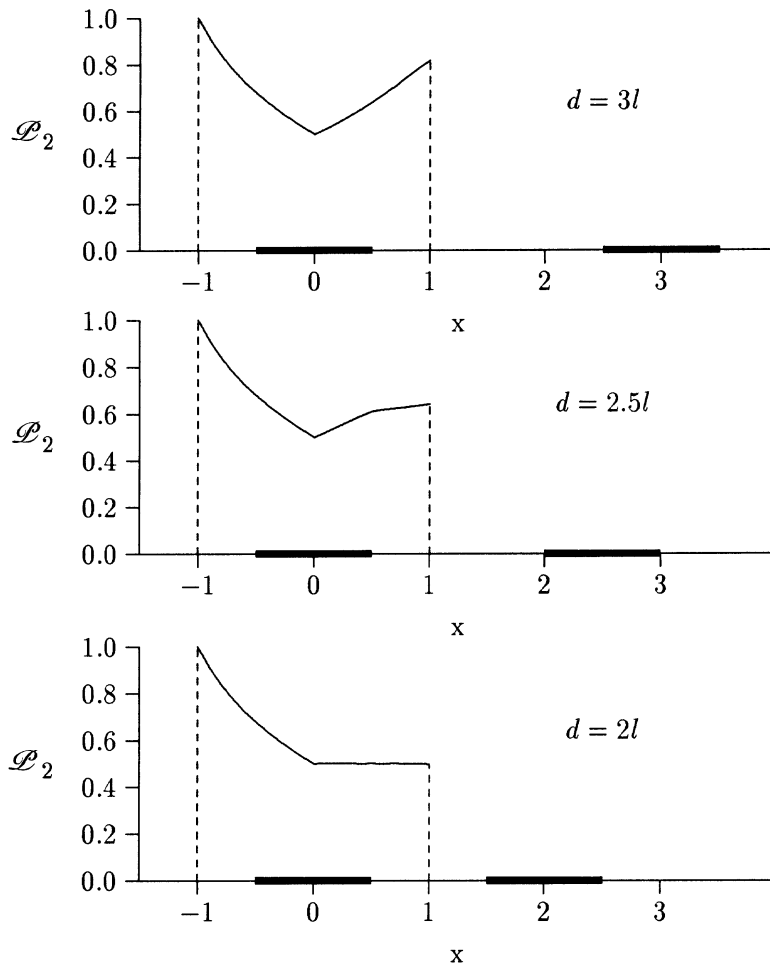


Fig. 7. - $\mathcal{P}_2(x)$ represents the probability density function to hit a particle in the presence of a nearby particle, located at a distance d .

results, some properties of the interior of a “fan”, obtained through the aggregation of square particles, of side l .

As we pointed out by the end of the preceding section, boundary growth is mainly due to the accretion of the boundary itself; nearby particles can be neglected, as they play a role only in 5% of cases. On the other hand, accretion laws of a particle in the interior are strongly influenced by the presence of nearby particles. This is pointed out in fig. 7, where $\mathcal{P}_2(x)$ is the probability density function for a particle to be hit in the position x , in the presence of a nearby particle, located at a distance d ; we notice that the probability density function $\mathcal{P}(x)$, discussed in the preceding section, differs from \mathcal{P}_2 because it represents the probability density for a particle to be hit in x and to become the more left particle (the new frontier particle on the left).

In the case of $d \gg l$, the chosen particle is essentially isolated, and the probability density function is symmetric with respect to $x = 0$; in this case the mean value of the

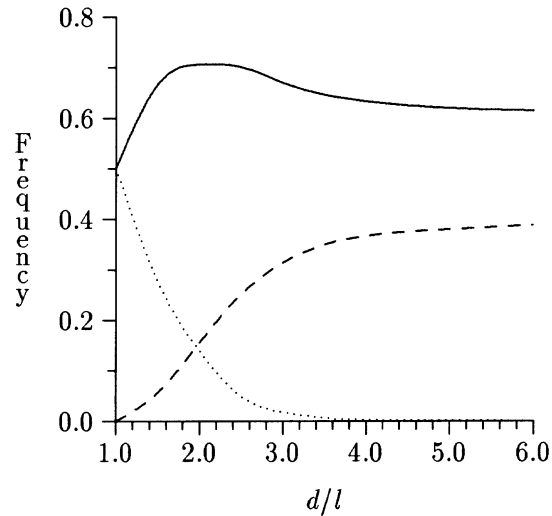


Fig. 8. – Frequency of three possible realizations, with 0 (dotted line), 1 (heavy line), or 2 particles (dashed line) directly connected with a seed, part of a horizontal line of infinite, equispaced seeds. The frequency is computed over ensemble averages of 10^5 aggregates.

number of particles, aggregating on the chosen particle, is larger than one, $\left(\int_{-1}^{+1} \mathcal{P}_2(x) dx = 1.39\right)$; this is due to those realizations collecting two particles. As d gets smaller, $d > 2l$, the nearby particle, together with its accretion “fan”, has a shadowing effect and the mean number of particles aggregating on the chosen particle becomes lower, but still larger than one (see fig. 7). As d gets even smaller, $d \leq 2l$, the value of the probability density function \mathcal{P}_2 stays constant, $\mathcal{P}_2 = 0.5$, the collection area also becomes smaller and the mean value of the number of particles aggregating on the chosen particle can get lower than one.

To retain a constant density in the average, each particle must collect exactly one particle; the previous argument implies that the average distance between particles must be $d = 2l$.

From a numerical calculation of the probability density function \mathcal{P}_2 run over a large set of aggregates, this function turns out not to be constant as the preceding analysis suggests, but it presents a minimum in the central part and two equal maxima at the boundaries. This difference is due to the fact that, in the preceding analysis, we start with particles on the same level.

To further quantify the influence of nearby particles, we consider the growth of an ideal situation with infinite equispaced seeds and we evaluate the distributions of particles directly connected with these seeds. Three realizations are possible with zero, one or two particles collected by the seed. Figure 8 shows the frequency of these realizations, computed over ensemble averages of 10^5 aggregates.

When particles are joined, $d/l = 1$, it is impossible to collect two particles; in 50% of cases one particle is collected and in the other 50% no particles are collected; in this case, each particle collects half particle on average and the particle density, propor-

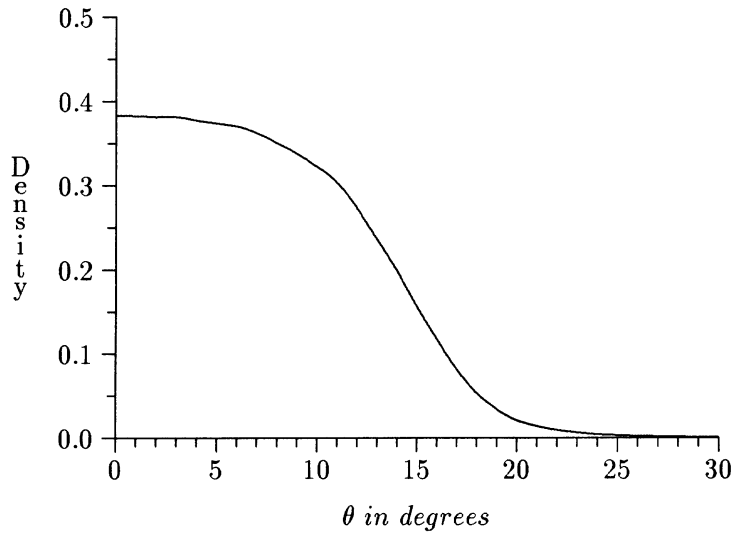


Fig. 9. – Mean density of a seed “fan”; θ is the angle between a considered line originating from the seed and its central one.

tional to the total number of particles of that line, is reduced to half on the next line. Here density represents the fraction of space occupied by particles.

Increasing the distance between seeds, the number of cases with zero particles collected rapidly decreases, while the number of cases with one or two particles collected increases. When d/l gets closer to 2, the number of cases with zero particles collected equals the number of cases with two particles collected; for this particular value of the ratio d/l , each particle collects one particle on average and the particle density stays constant on the next line.

It is interesting to notice that, running a statistical calculation over a large set of aggregates, we get that each particle collects 0 particles in 17% of cases, 1 particle in 66% of cases, 2 particles in 17% of cases; these values are very similar to fig. 8 values.

Increasing the distance beyond this value, $d/l > 2$, the number of cases with zero particles collected keeps decreasing, while the numbers of cases with one and two particles collected become constant. For these values of the ratio, each particle collects more than one particle on average and the particle density increases on the next line.

The case in which the density is constant, d/l close to 2, represents a stable equilibrium for our system, with a density value close to 0.5.

This result is similar to the previous one, obtained with a single nearby particle; this shows that all other particles of the line play a minor role.

This density value of 0.5 is larger than the value of 0.38, observed near the center of the “fan” (see fig. 9); these differences should be attributed to the presence of regions with empty channels, with zero density, due to the shadowing effect that will be discussed later. Instead, in the preceding theoretical section, the considered region is assumed to be uniformly occupied by particles.

Figure 9 is obtained through ensemble averages of 10^6 aggregates; the density

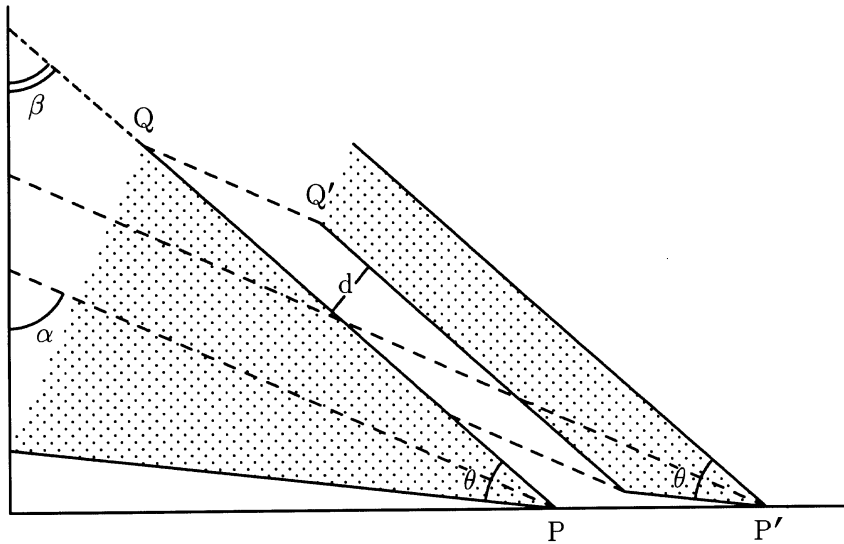


Fig. 10. - Two-seeds growing evolution scheme with d width channel formation, due to shadowing effects. P and P' are point seeds, Q is a point at the left boundary and Q' is its shadow, θ is the opening angle of the fan, α is the angle that gives the direction of incoming particles and β is the angle that gives the direction of the empty channel.

mean value is constant on each line originating from the seed and it is symmetrical with respect to the central line, which goes through the seed along the direction of falling particles. The density values of these lines are shown in fig. 9, where θ is the angle between the considered line and the central one. Density variations do not correspond to density variation in the single aggregates but to differences in their geometric shape; the density is about constant in each aggregate till its edge, where it vanishes abruptly in few particles.

5. - Air inclusion channels

A distinct columnar morphology is evident in bidimensional simulations, see Meakin *et al.* [16], and in real experiments, see Ramanlal and Sander [3]. These columnar structures are clear and become clearer with the increase of the angle of incidence.

In this section, we propose a law for the angle of growth of the columnar structures observed both in real experiments and in numerical simulations; this law is supported by the following argument based on the contemporary accretion of two seeds.

In fig. 10, we consider some random uniformly distributed particles, moving along parallel trajectories, toward two point seeds. Both seeds develop their "fan" independently, till the P fan starts shadowing the P' fan and, in particular, the point Q' is shadowed by the point Q . Then, as fans keep growing, Q moves on the right boundary of the P fan and its shadow Q' moves with the same speed on the P' fan, defining its left boundary. This argument implies that P' fan left boundary grows together with P fan right boundary and a channel is formed; the width and the

direction of the channel are, respectively, given by

$$d = \overline{PP'} \sin(\alpha) \sin(\alpha - \beta), \quad \beta = \alpha - \theta/2,$$

where θ is the opening angle of the fan, see fig. 10. This law explains the relation between the direction of incoming particles (α) and the direction of the empty channels (β) present in the interior of the aggregates; in particular it shows how the channels have generally the same “fan-opening angle”. This has been shown in two-dimensional numerical aggregates, see Porcú and Prodi [7], and in tridimensional laboratory and numerical aggregates, see Ramanlal and Sander [3].

We notice how our law agrees with eq. (8) of Meakin *et al.* and our argument supports their empirical law. Our law explains the experimental data of table I of Meakin *et al.*; the agreement is quite good for large angles of incidence, when channels are well defined; for medium and small angles of incidence, the agreement is much better than the tangent rule predictions, even if the calculation of β is ambiguous.

REFERENCES

- [1] VOLD M. J., *J. Colloid. Sci.*, **18** (1963) 684.
- [2] EDEN M., *Proc. Fourth Berkeley Symp. Math. Stat. Prob.*, **4** (1961) 223.
- [3] RAMANLAL P. and SANDER L. M., *Phys. Rev. Lett.*, **54** (1985) 1828.
- [4] LIMAYE A. V. and AMRITKAR R. E., *Phys. Rev. A*, **34** (1986) 5085.
- [5] RAMBALDI S., PRODI F. and PORCÚ F., *Proceedings of the VI International Conference on Atmospheric Icing of Structures, Paris, 1988* (J.-L. Quinet E. d. F., Paris, France) 1988.
- [6] LIANG S. and KADANOFF L. P., *Phys. Rev. A*, **31** (1985) 2628.
- [7] PORCÚ F. and PRODI F., *Phys. Rev. A*, **44** (1991) 8313.
- [8] BUSER O. and AUFDERMAUR A. N., *Q. J. R. Meteorol. Soc.*, **99** (1973) 388.
- [9] PRODI F., SMARGIASSI E. and PORCÚ F., *Atmos. Res.*, **32** (1994) 95.
- [10] PORCÚ F., SMARGIASSI E. and PRODI F., *Atmos. Res.*, **36** (1995) 233.
- [11] LOZOWSKI E. P., STALLABRASS J. R. and HEARTHY P. F., *J. Clim. Appl. Meteorol.*, **22** (1983) 2053.
- [12] LOZOWSKI E. P., STALLABRASS J. R. and HEARTHY P. F., *J. Clim. Appl. Meteorol.*, **22** (1983) 2063.
- [13] SZILDER K., *Q. J. R. Meteorol. Soc.*, **119** (1993) 907.
- [14] PRODI F., LEVI L. and PEDERZOLI P., *Q. J. R. Meteorol. Soc.*, **112** (1986) 1081.
- [15] JOAG P. S., LIMAYE A. V. and AMRITKAR R. E., *Phys. Rev. A*, **36** (1987) 3395.
- [16] MEAKIN P., RAMANLAL P., SANDER L. M. and BALL R. C., *Phys. Rev. A*, **34** (1986) 5091.